# Observation of magnons in $Mn_2Au$ films by inelastic Brillouin and Raman light scattering

M. Arana, F. Estrada, D. S. Maior, J. B. S. Mendes, L. E. Fernandez-Outon, W. A. A. Macedo, V. M. T. S. Barthem, D. Givord, A. Azevedo, and S. M. Rezende

Citation: Appl. Phys. Lett. **111**, 192409 (2017);
View online: https://doi.org/10.1063/1.5001705
View Table of Contents: http://aip.scitation.org/toc/apl/111/19
Published by the American Institute of Physics



# Observation of magnons in $Mn_2Au$ films by inelastic Brillouin and Raman light scattering

M. Arana,[1,2] F. Estrada,[1,3] D. S. Maior,[1] J. B. S. Mendes,[4] L. E. Fernandez-Outon,[5,6] W. A. A. Macedo,[6] V. M. T. S. Barthem,[2] D. Givord,[2,7] A. Azevedo,[1] and S. M. Rezende[1]
[1]*Departamento de Física, Universidade Federal de Pernambuco, 50670-901 Recife, PE, Brazil*
[2]*Instituto de Física, Universidade Federal do Rio de Janeiro, 21941-909 Rio de Janeiro, RJ, Brazil*
[3]*Facultad de Biología, Universidad Michoacana de San Nicolás de Hidalgo, Av. F. J. Mújica s/n, 58030 Morelia, Michoacán, Mexico*
[4]*Departamento de Física, Universidade Federal de Viçosa, 36570-900 Viçosa, MG, Brazil*
[5]*Departamento de Física, Universidade Federal de Minas Gerais, 31270-901 Belo Horizonte, MG, Brazil*
[6]*Centro de Desenvolvimento da Tecnologia Nuclear, CDTN, 31270-901 Belo Horizonte, MG, Brazil*
[7]*CNRS/Université Grenoble Alpes, Institut Néel, F-38000 Grenoble, France*

(Received 25 August 2017; accepted 14 October 2017; published online 8 November 2017)

The intermetallic antiferromagnetic compound $Mn_2Au$ has been attracting considerable interest for antiferromagnetic spintronics due to its high Néel temperature and strong spin–orbit coupling. We report on the experimental investigation of the zero-wave number magnon frequencies in $Mn_2Au$ films using Brillouin and Raman inelastic light scattering techniques. The derived effective anisotropy field values are in close agreement with theoretical calculations. With the values of the anisotropy and exchange fields, the full magnon dispersion curves in $Mn_2Au$ were calculated. Due to the weak in-plane anisotropy, the $k \sim 0$ frequency of the lower magnon branch, 121 GHz, is among the lowest for 3D antiferromagnets, suggesting that $Mn_2Au$ is a good candidate for realizing the generation of spin currents by antiferromagnetic resonance driven spin-pumping, as proposed theoretically. *Published by AIP Publishing*. https://doi.org/10.1063/1.5001705

Since the discovery of giant magnetoresistance (GMR) in 1988, spintronics, the field of electronics that incorporates the electron spin, has almost uniquely exploited the properties of ferromagnetic materials.[1] In spintronic devices, antiferromagnetic materials (AFMs) play only the passive role of freezing the orientation of the ferromagnetic moments in the pinned layer of GMR or TMR (tunnel magnetoresistance) spin-valve trilayers. Despite a number of attractive properties (AFMs do not generate stray magnetic fields and are not affected by the presence of other AFM elements in their surrounding), the incorporation of AFM materials in spintronic devices raises specific difficulties. In particular, the lack of stray field implies that reading information written in an AFM element requires specific probes. Additionally, the magnetic state of AFM materials cannot be controlled via magnetic fields. Until now, this property was thought to preclude the use of AFM materials as active elements of any spintronic devices. However, recent theoretical studies demonstrated that the orientation of AFM moments should be controllable via spin-orbit torque (SOT).[2] This result has attracted considerable interest towards AFM materials for AFM spintronics.[3] Note also that (i) AFMs have ultrafast dynamical response with frequencies on the order of THz,[4,5] higher than those of FM (GHz)[6,7] because the AFM moments of one sublattice precess about the exchange field due to exchange interactions with the moments on the other sublattice and that (ii) AFM materials with strong spin-orbit coupling (SOC) are potential candidates for converting spin currents into charge currents by the inverse spin Hall effect (ISHE).[8,9]

The progressive understanding that AFM materials may have high potential for spintronic applications has stimulated the search for new materials with high SOC and therefore potentially large spin Hall effect and the exhaustive characterization of the associated spin configuration and spin dynamics (CuMnAs, IrMn).[2,8] In this category of AFM materials, $Mn_2Au$ has been predicted theoretically[10,11] and experimentally confirmed to exhibit very attractive properties.[12] The magnetic structure of $Mn_2Au$ is formed of ferromagnetic sheets, stacked along the c-axis of the tetragonal structure, with the orientation of the moments alternating from one sheet to the next. The Néel temperature of $Mn_2Au$ is very high, $T_N \approx 1350$ K. The Mn moments are confined to the (001) plane by large second order anisotropy,[13] and the in-plane easy direction of the moment is [110] as defined by the 4-fold anisotropy.[13] This suggests the possible occurrence of large tunnel anisotropic magnetoresistance (TAMR) effects.

One of the methods proposed to generate spin currents in AFM materials is spin-pumping driven by antiferromagnetic resonance,[14] which corresponds to the generation of zero wave number magnons. In this study, we report the observation of magnons in $Mn_2Au$ films (100 nm-thick) by inelastic Brillouin and Raman light scattering, and we calculate the full dispersion relation using the anisotropy field values obtained from the measured magnon frequencies.

$Mn_2Au$ is the Mn richest of all Mn-Au compounds. It forms by peritectic reaction at 660 °C and decomposes above 680 °C into pure Mn and equiatomic MnAu. In bulk, the compound may be obtained by mixing the proper amount of Mn and Au and annealing at a temperature close to but below 680 °C. Epitaxial (101) films were obtained by growth on (001) MgO,[15] whereas epitaxial (001) films were obtained by Jourdan *et al.*[16] on (1-102) $Al_2O_3$. Polycrystalline films of

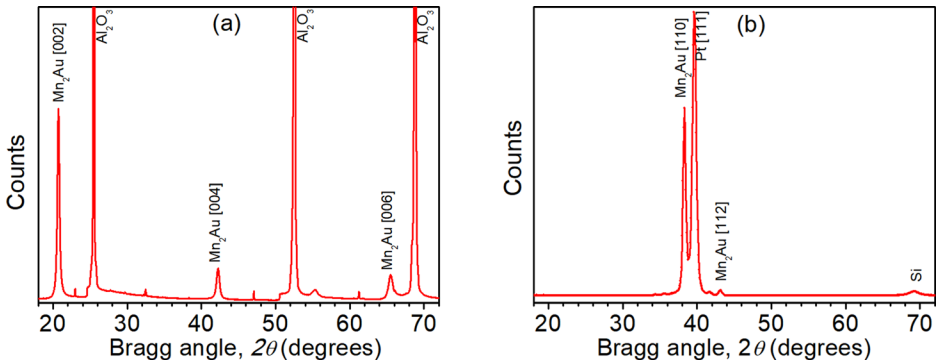


FIG. 1. XRD patterns of 100 nm thick (001) and (110) $Mn_2Au$ films: (a) $Al_2O_3/Mn_2Au(100\,nm)/Ta(3\,nm)$; (b)$Si/SiO_2/Pt(24\,nm)/Mn_2Au(100\,nm)/Ta(3\,nm)$.

$Mn_2Au$, of typical thickness 10–25 nm, have been obtained as well as textured (110) $Mn_2Au$ films on (111) Pt (in preparation).

In the present study, we have used two procedures to prepare films of $Mn_2Au$. In the first, a PVD magnetron sputtering tool was used for the growth of the (001) $Mn_2Au$ film. For this purpose, Mn and Au were co-deposited at 600 °C directly onto the $Al_2O_3$(1-102) substrate. After deposition, a 3 nm Ta capping layer was used to prevent oxidation and deterioration, resulting in a sample structured as follows: $Al_2O_3/Mn_2Au/Ta$. As seen in Fig. 1(a), XRD peaks appear at $2\theta = 20.89°$, 42.30°, and 65.54° corresponding to the (002), (004), and (006) $Mn_2Au$ Bragg reflections. The derived preferential orientation with the [001] direction perpendicular to the film surfaces is in accordance with Ref. 16. In the second procedure, a 100 nm-thick (110)-textured $Mn_2Au$ film was prepared by combining sputtering from a $Mn_2Au$ target and evaporation from a Mn Knudsen cell. The substrate was surface-oxidized (100) Si onto which a 3 nm-thick Ta seed layer and a 24 nm-thick (111) Pt layer were deposited prior to Mn/Au deposition. Films obtained by sputtering from the $Mn_2Au$ target only were found to exhibit the equiatomic MnAu phase. An additional Mn layer was required to obtain the desired $Mn_2Au$ phase. This was evaporated from the Knudsen cell. A 4 nm-thick Ta layer was deposited on top of the whole stack to avoid oxidation. The sample was annealed at 350 °C for 1 h followed by 480 °C for 5 h. The structural characterization was done with the aid of a D2 PHASER 2nd generation benchtop X-Ray diffractometer using the Cu K-α radiation ($\lambda = 1.5418$ Å). Figure 1(b) shows the theta/2theta X-Ray diffraction (XRD) peak of the $Mn_2Au$ (110) plane at 38.29° and Pt(111) at 39.65°. No peaks corresponding to MnO or MnAu were detected by XRD. Both samples were used for the analysis of the magnon behavior.

We performed inelastic Brillouin (BLS) and Raman light scattering experiments to study the zone-center magnons in $Mn_2Au$. Both BLS and Raman light scattering are versatile techniques, and it has been widely demonstrated that these provide information on the dispersion relation of materials in a very broad range of magnon frequencies.[17–21]

The BLS measurements were carried out on the $Mn_2Au$ films of both orientations at room temperature using the backscattering geometry. The samples having a $5 \times 5\,mm^2$ surface area were mounted between the poles of an electromagnet with a magnetic field, $\mu_0 H_0$, of 0.1 T in the film plane. In the equipment used, the light source is a single-mode-stabilized Spectra Physics diode laser operating at 532 nm, with a power of 300 mW. This power is attenuated by filters, and the power impinging on the sample is reduced to 33 mW. The laser beam is focused on the film surface by an f/1.7 camera lens, with the plane of incidence normal to both the film plane and the field. For both films during the BLS experiments, the samples were positioned at different incidence angles (35° and 65° for 110 and 001 films, respectively). The scattered radiation collected and collimated by the same lens passes through an analyzer with the axis at 90° to the laser polarization, and it is then directed and focused to the entrance pinhole of a Fabry-Perot interferometer to be frequency analyzed. The interferometer is a Sandercock TFP-1 tandem system operating in a $(2 \times 3)$-pass configuration, with automatic control and data acquisition made with a TFPDAS4 interface board and software package. The interface is connected directly to the low-noise solid-state Hamamatsu photodetector. Figure 2 shows a spectrum of the $Mn_2Au$ (110) film collected by averaging over 15 000 scans, using a free spectral range of 250 GHz, with noise reduction made by numerically averaging over 5 points and division by a function proportional to the fit to the Rayleigh light signal. The bumpy background is due to the averaging of the noise arising in the 5 h accumulation necessary to reveal the weak magnon peaks. These are identified by the Stokes and anti-Stokes lines with a frequency shift of 121 GHz, clearly seen in the spectrum of Fig. 2, which are attributed to the $k \sim 0$ low energy magnon in $Mn_2Au$. The applied field value 0.1 T in our work was enough to hopefully orient possible spin domains along a common direction and achieve the desired ordering and at the same time without much change in the magnon frequencies. Similar results were obtained in the $Mn_2Au$ (001) film.

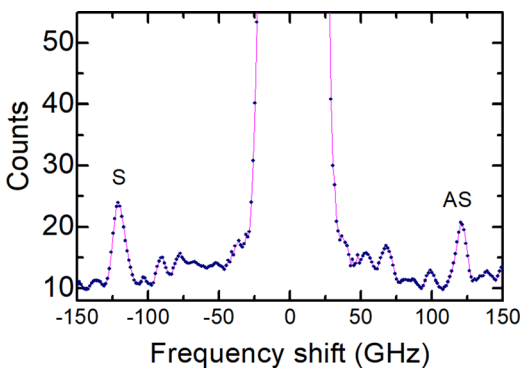


FIG. 2. BLS spectrum of the $Mn_2Au$ (110) film in a field of $\mu_0 H_0 = 0.1$ T showing the $k \sim 0$ thermal magnon Stokes (S) and anti-Stokes (AS) lines with a frequency shift of 121 GHz.

The Raman spectra of the $Mn_2Au$ films were collected with a Renishaw In Via micro-Raman system equipped with a 514.5 nm argon laser line and with a 785 nm diode laser. The measurements were performed with all available laser lines at different points of the sample surface using a long distance 50× objective lens, resulting in a laser spot having a diameter around 1 $\mu$m in the focal plane. The laser excitation powers in the sample surface were 150 and 0.9 mW when using the diode or the argon laser, respectively. High pass filters were used to attenuate the elastically scattered light along the laser line direction. The spectra obtained under various conditions exhibit several lines in the range of 3–9 THz arising from magnons in the $Mn_2Au$ film and phonons generated within all layers of the sample and in the substrate. When the crossed polarizer and analyzer are introduced intercepting either the laser path or the scattered light beam, two Raman shifted lines are consistently less attenuated than the others, the one at 3.24 THz and the other at 4.2 THz. These lines are attributed to magnons in $Mn_2Au$. This is so because the light scattered by magnons is circularly polarized[17] while the light originating from phonons is linearly polarized. Figure 3 shows a spectrum of the $Mn_2Au$ (001) film obtained with the 785 nm (infrared) diode laser line, with a noise reduction scheme made by numerically averaging over 5 points and subtraction by a function proportional to the background scattered light. Similar results were obtained in the $Mn_2Au$ (110) film as expected.

As discussed above, $Mn_2Au$ is a two-sublattice antiferromagnet with Néel temperature $T_N \approx 1350$ K. The Mn spins are confined in the (001) plane of the tetragonal structure by a large magnetocrystalline anisotropy; within this plane, they lie along the easy [110] direction.[13] Here, we will ignore the existence of a small orthorhombic distortion occurring below $T_N$ (see below) and consider the spins in neighboring (001) planes oppositely aligned forming a two sublattice AFM arrangement. The spin Hamiltonian with Zeeman energy, exchange interaction, and out-of-plane (x) and in-plane (y,z) anisotropy energies can be written as

$$\mathrm{H} = -\gamma\hbar \sum_{i,j} H_0 S^z_{i,j} + \sum_{i,j} 2J_{ij}\,\vec{S}_i \cdot \vec{S}_j + \sum_i D_1 (S^x_1)^2 + \frac{D_2}{S^2}(S^y_i)^2 (S^z_i)^2, \quad (1)$$

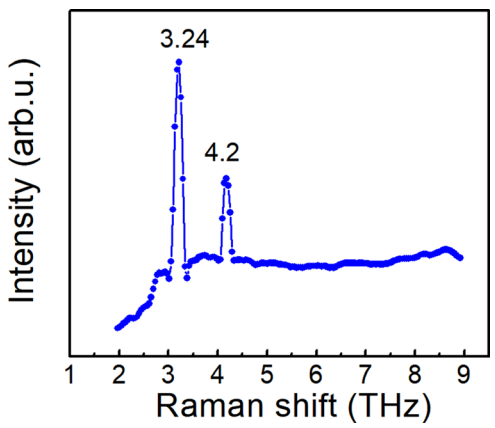


FIG. 3. Raman shift spectrum of the $Mn_2Au$ (001) film showing two k ∼ 0 thermal magnon lines at 3.24 and 4.2 THz.

where $\vec{S}_i$ and $\vec{S}_j$ are the spins (in units of $\hbar$) at sites $i$ and $j$ of sublattices 1 and 2, respectively, $H_0$ is the applied static magnetic field, $J_{ij}$ is the exchange constant representing the interaction between spins $\vec{S}_i$ and $\vec{S}_j$, $\mu_0$ is the vacuum permeability, $\gamma = g\mu_B/\hbar$ is the gyromagnetic ratio, $g$ is the spectroscopic splitting factor, $\mu_B$ is the Bohr magneton, $\hbar$ is the reduced Planck constant, $D_1 > 0$ is the anisotropy constant along the [001] hard direction, $x$, and $D_2 > 0$ is the anisotropy constant along both easy directions, $y$ and $z$, the $\langle 110 \rangle$ perpendicular axes, with $D_1$ and $D_2$ in Joules. The Hamiltonian in Eq. (1) has a similar form to the one for the hard-axis room temperature NiO[7,22] except for the last term expressing the in-plane anisotropy in $Mn_2Au$. The energy operator of Eq. (1) was treated with a second quantization formalism by which the spin operators for the two sublattices are first transformed into collective boson operators and then into magnon creation and annihilation operators $\alpha^\dagger_k, \alpha_k, \beta^\dagger_k, \beta_k$. Neglecting magnon interactions, the quadratic Hamiltonian in Eq. (1) is cast in the diagonal form

$$\mathrm{H} = \sum_k \hbar\,(\omega_{\alpha k}\,\alpha^+_k \alpha_k + \omega_{\beta k}\,\beta^+_k \beta_k), \quad (2)$$

where $\omega_{\alpha k}$ and $\omega_{\beta k}$ are the frequencies of the two magnon modes. Following Ref. 7, one can show that the unrenormalized magnon frequencies for $H_0 = 0$ are

$$\omega^2_{\alpha k} = A^2_k - (B_k - C_k)^2, \quad (3)$$

$$\omega^2_{\beta k} = A^2_k - (B_k + C_k)^2, \quad (4)$$

where

$$A_k = \mu_0\gamma\,[H_E + (H_{A1} + H_{A2})/2], \quad (5)$$

$$B_k = \mu_0\gamma\gamma_k H_E, \quad (6)$$

$$C_k = \mu_0\gamma(H_{A1} - H_{A2}), \quad (7)$$

where $H_E$, $H_{A1}$, and $H_{A2}$ are the effective exchange and anisotropy fields defined by

$$H_E = 2\,\mathrm{SzJ}/g\mu_0\mu_B, \quad H_{A1} = 2S\,D_1/g\mu_0\mu_B, \quad H_{A2} = 2S\,D_2/g\mu_0\mu_B, \quad (8)$$

where, in accordance with the theoretical calculations,[9] we have considered only intersublattice exchange interaction between the $z$ nearest neighbors with parameter $J$ and relative position vectors $\vec{\delta}$, such that

$$\gamma_k = (1/z)\sum \exp\left(i\vec{k}.\vec{\delta}\right) \quad (9)$$

is a geometrical factor. As shown in Ref. 7, the magnon frequencies vary with the square of the magnetic field, so that at low fields one can neglect the effect of the field. Using the relations (5)–(8) in Eqs. (3) and (4), one can write the frequencies of the two magnon modes in terms of the effective fields

$$\omega^2_{\alpha k} = (\mu_0\gamma)^2[H_E(H_{A1} + H_{A2}) + H_{A1}H_{A2} + \gamma_k H_E(H_{A1} - H_{A2}) + H^2_E(1 - \gamma^2_k)], \quad (10)$$

$$\omega_{\beta k}^2 = (\mu_0\gamma)^2[H_E(H_{A1}+H_{A2}) + H_{A1}H_{A2} - \gamma_k H_E(H_{A1}-H_{A2}) + H_E^2(1-\gamma_k^2)]. \quad (11)$$

The frequencies of the zone-center $k \approx 0$ modes, corresponding to the magnons probed by one-magnon light scattering, with $\gamma_k = 1$ and with $H_E \gg H_{A1} \gg H_{A2}$, Eqs. (10) and (11), give

$$\omega_{\alpha 0} \approx (\mu_0\gamma)(2H_{A1}H_E)^{1/2}, \quad (12)$$

$$\omega_{\beta 0} \approx (\mu_0\gamma)(2H_{A2}H_E)^{1/2}. \quad (13)$$

The exchange field for $Mn_2Au$, derived from susceptibility measurements, is around $\mu_0 H_E = 1300$ T,[12] and considering the $g$-factor for the Mn moments $g = 2.0$, the gyromagnetic ratio is $\gamma = 28$ GHz/T. Using these numbers and the frequency of the lower branch $k \approx 0$ magnon mode, measured by BLS, $f_{\beta 0} = \omega_{\beta 0}/2\pi = 121$ GHz, we obtain with Eq. (13) for the in-plane anisotropy field $\mu_0 H_{A2} = 0.007$ T which is comparable to the theoretical estimate.[11] In regard to the magnons in the upper energy branch, the fact that we have observed two lines in the Raman spectrum indicates the presence of a small orthorhombic distortion in the AFM phase of $Mn_2Au$, which can be attributed to magnetostriction. The distortion lifts the equivalence of some spin sites ensuring that there are actually four spin sublattices and correspondingly four magnon modes, similar to NiO.[17,20] Since we are using a two spin-sublattice approximation, we assumed in the analysis of the Raman data that the frequency of the upper branch $k \approx 0$ magnon mode is the average of the two measured values, 3.72 THz. Using this value in Eq. (11) and the same exchange field and $g$-factor, we obtain for the hard axis anisotropy field $\mu_0 H_{A1} = 5.3$ T, which is also comparable to the theoretical estimate.[11] The full magnon dispersion relations, calculated using the obtained anisotropies field values, are shown in Fig. 4. Figure 4(a) shows the full magnon dispersion relations for $Mn_2Au$ calculated with Eqs. (9) and (10), using the values for the effective fields $\mu_0 H_E = 1300$ T and $\mu_0 H_{A2} = 0.0072$ T assuming a spherical Brillouin zone and using for the structure factor $\gamma_k = \cos(\pi k/2k_m)$, where $k_m = \pi/a_l$, with $a_l$ being the lattice parameter.

In conclusion, the magnon frequencies corresponding to the k ∼ 0 wave vector were measured by Brillouin light scattering at 121 GHz and by Raman spectroscopy at around 3.72 THz in films of antiferromagnetic $Mn_2Au$ with (110) and (001) orientations. The full dispersion relation was calculated using a spin Hamiltonian considering the Zeeman energy, the exchange interaction, and the out-of-plane and in-plane anisotropy energies. The resulting calculated hard anisotropy field amounts to 5.3 T and that of the in-plane anisotropy to 0.007 T. Knowledge of the lowest magnon frequency in $Mn_2Au$, 121 GHz at low fields, suggests that this compound is a more convenient candidate to achieve spin current generation by spin pumping through antiferromagnetic resonance (AFMR) than the AFMs considered in Ref. 4. $MnF_2$ and $FeF_2$ have the lowest magnon frequencies at, respectively, 260 GHz[14,23] and 1.56 THz.[24] The observation of such high frequency magnons involves difficult AFMR techniques. It also requires working at low temperatures, since $MnF_2$ and $FeF_2$ order below room temperature, as well as the application of high magnetic fields to separate the magnon branches.[14,23,24] In contrast, $Mn_2Au$ is AFM ordered at room temperature and the magnon branches are separated even at low fields.

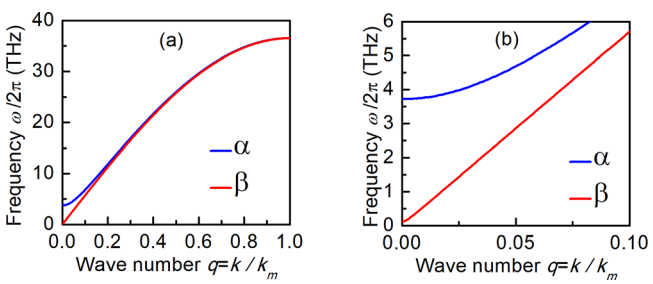


FIG. 4. (a) Magnon frequencies versus wave number in antiferromagnetic $Mn_2Au$ calculated with Eqs. (9) and (10) assuming a spherical Brillouin zone. (b) Blow up of the Brillouin zone center showing the separation of the frequencies of the α (upper blue curve) and β (lower red curve) magnon modes.

This research was supported by Conselho Nacional de Desenvolvimento Científico e Tecnológico (CNPq), Coordenação de Aperfeiçoamento de Pessoal de Nível Superior (CAPES), Financiadora de Estudos e Projetos (FINEP), Fundação de Amparo à Ciência e Tecnologia do Estado de Pernambuco (FACEPE) and Fundação de Amparo à Pesquisa do Estado de Minas Gerais (FAPEMIG) in Brazil, and by Consejo Nacional de Ciencia y Tecnología (CONACYT) in Mexico. Authors M. Arana and F. Estrada thank CNPq for the Grant of a Post-Doctoral fellowship associated to this project.

[1]I. Žutić, J. Fabian, and S. Das Sarma, Rev. Mod. Phys. **76**, 323 (2004).
[2]P. Wadley, B. Howells, J. Železný, C. Andrews, V. Hills, R. P. Campion, V. Novák, K. Olejník, F. Maccherozzi, S. S. Dhesi, S. Y. Martin, T. Wagner, J. Wunderlich, F. Freimuth, Y. Mokrousov, J. Kuneš, J. S. Chauhan, M. J. Grzybowski, A. W. Rushforth, K. W. Edmonds, B. L. Gallagher, and T. Jungwirth, Science **351**, 587 (2016).
[3]T. Jungwirth, X. Marti, P. Wadley, and J. Wunderlich, Nat. Nanotechnol. **11**, 231 (2016).
[4]R. Cheng, J. Xiao, Q. Niu, and A. Brataas, Phys. Rev. Lett. **113**, 057601 (2014).
[5]Y. Mukai, H. Hirori, T. Yamamoto, H. Kageyama, and K. Tanaka, Appl. Phys. Lett. **105**, 022410 (2014).
[6]T. Kampfrath, A. Sell, G. Klatt, A. Pashkin, S. Mährlein, T. Dekorsy, M. Wolf, M. Fiebig, A. Leitenstorfer, and R. Huber, Nat. Photonics **5**, 31 (2011).
[7]S. M. Rezende, R. L. Rodríguez-Suarez, and A. Azevedo, Phys. Rev. B **93**, 054412 (2016); F. L. A. Machado, P. R. T. Ribeiro, J. Holanda, R. L. Rodríguez-Suárez, A. Azevedo, and S. M. Rezende, Phys. Rev. B **95**, 104418 (2017).
[8]J. B. S. Mendes, R. O. Cunha, O. Alves Santos, P. R. T. Ribeiro, F. L. A. Machado, R. L. Rodríguez-Suárez, A. Azevedo, and S. M. Rezende, Phys. Rev. B **89**, 140406 (2014).
[9]W. Zhang, M. B. Jungfleisch, W. Jiang, J. E. Pearson, A. Hoffmann, F. Freimuth, and Y. Mokrousov, Phys. Rev. Lett. **113**, 196602 (2014).
[10]S. Khmelevsky and P. Mohn, Appl. Phys. Lett. **93**, 162503 (2008).
[11]A. B. Shick, S. Khmelevskyi, O. N. Mryasov, J. Wunderlich, and T. Jungwirth, Phys. Rev. B **81**, 212409 (2010).
[12]V. M. T. S. Barthem, C. V. Colin, H. Mayaffre, M. H. Julien, and D. Givord, Nat. Commun. **4**, 2892 (2013).
[13]V. M. T. S. Barthem, C. V. Colin, R. Haettel, D. Dufeu, and D. Givord, J. Magn. Magn. Mater. **406**, 289 (2016).
[14]P. Ross, M. Schreier, J. Lotze, H. Huebl, R. Gross, and S. T. B. Goennenwein, J. Appl. Phys. **118**, 233907 (2015).
[15]M. Meinert, D. Graulich, and T. Matalla-Wagner, e-print arXiv:1706.06983 [cond-mat.mtrl-sci].

[16]M. Jourdan, H. Bräuning, A. Sapozhnik, H.-J. Elmers, H. Zabel, and M. Kläui, J. Phys. D: Appl. Phys. **48**, 385001 (2015).
[17]M. G. Cottam and D. J. Lockwood, *Light Scattering in Magnetic Solids* (J. Wiley & Sons, New York, 1986).
[18]J. Milano, L. B. Steren, and M. Grimsditch, Phys. Rev. Lett. **93**, 077601 (2004).
[19]J. Zhao, A. V. Bragas, R. Merlin, and D. J. Lockwood, Phys. Rev. B **73**, 184434 (2006).
[20]M. Grimsditch, L. E. McNeil, and D. J. Lockwood, Phys. Rev. B **58**, 14462 (1998).
[21]M. M. Lacerda, F. Kargar, E. Aytan, R. Samnakay, B. Debnath, J. X. Li, A. Khitun, R. K. Lake, J. Shi, and A. A. Balandin, Appl. Phys. Lett. **110**, 202406 (2017).
[22]M. T. Hutchings and E. J. Samuelsen, Phys. Rev. B **6**, 3447 (1972).
[23]R. W. Sanders, D. Paquette, V. Jaccarino, and S. M. Rezende, Phys. Rev. B **10**, 132 (1974).
[24]R. W. Sanders, V. Jaccarino, and S. M. Rezende, Solid State Commun. **28**, 907 (1978).